Plasmonic-heating-induced Nanofabrication on Glass Substrates

View Article Online
DOI: 10.1039/C6NR06543K

*Yuki Osaka, Satoshi Sugano and Shuichi Hashimoto**

Department of Optical Science and Technology, University of Tokushima, 2-1 Minami-Josanjima, Tokushima 770-8506, Japan.

E-mail: hashichem@tokushima-u.ac.jp

Electronic supplementary information (ESI) available. See DOI:

Particle image and histogram, nanohole fabrication on a silica glass, particle temperature estimation, numerical simulation of optical spectra.

Table of content entry:

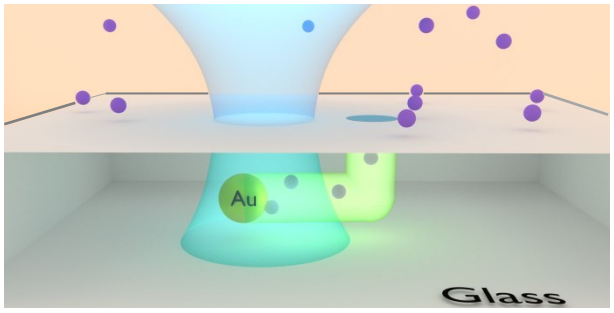

Plasmonic heating embeds a single gold nanoparticle and bores a nanocavity into the glass substrate

View Article Online
DOI: 10.1039/C6NR06543K

Abstract: Fabricating nano-sized through-holes on a coverslip approximately 100 μm thick is challenging but rewarding when applied to ultrafine filters that separate proteins and DNA of various sizes and isolate viruses from cells. Toward this end, we developed an *in situ* etching-assisted laser processing technique exploiting gold nanoparticles. Plasmonic heating of a single gold nanoparticle through focused illumination of a continuous-wave laser beam enables structural modifications to be localized to the contact area on the glass surface. This results in the embedding of the particle forming nanocavities caused by chemical etching with aqueous tetrabutylammonium hydroxide. Depending on the shape of the nanoparticle, a highly flexible face geometry design such as a disk and triangle was achieved. The etching was monitored *in situ* through measurements of spectral red shifts in single-particle scattering, indicating an increasing medium refractive index consistent with embedding. The embedding process is unexpectedly fast, at 0.8 μm with 5 minutes of illumination. Besides nanoholes, we fabricated nanodomes around a single gold nanoparticle supported on a glass substrate through laser-heating-induced encapsulation. Overall, we were able to demonstrate true nano-laser processing free from diffraction-limited optics, with potential benefits of simple low-cost fabrication.

Introduction

Gold nanoparticles (Au NPs) are characterized by their localized surface plasmon resonance (LSPR), which is a coherent oscillation of the conduction electrons initiated by their interaction with visible and near-infrared light.[1] The LSPR of plasmonic nanoparticles has attracted considerable interest recently because of noted applications in various fields such as sensing,[2,3] photocatalysis,[4,5] and light energy conversion.[6] The LSPR decays both radiatively and nonradiatively; whereas the former is responsible for the plasmonic enhancement of the electric field in the near-field regime,[1] the latter generates hot electrons that eventually lead to particle heating.[7] This is the origin of the photothermal response. The photothermal effect of plasmonic nanoparticles or, in short, plasmonic heating has gained research recognition through intriguing applications such as nanoheaters,[8,9] photothermal image enhancers,[10,11] and vapor nanobubble generators.[12,13]

Plasmonic heating of Au NPs has potential applications in nanostructuring and nanofabrication. For instance, nanopatterning the surfaces of polymer film induced by a single Au NP has been demonstrated. A tightly focused laser beam exerting an optical force onto an NP simultaneously with optical heating was used to move it inside the film, causing melting and thermal decomposition of the polymer to form grooves.[14] Plasmonic heating was also used to control nanoscale thermal curing of polydimethylsiloxane to synthesize nanoparticles and nanowires.[15] By contrast, nanoscale structuring and processing with glass substrates are considerably challenging but practically useful for chemical-resistant ultrafine filters for separating proteins, DNA, and viruses. For this purpose, mere optical heating applied to polymer films has little use; it is not feasible to maintain particle temperatures high enough to melt glass around the particle without causing particle evaporation and fragmentation.[16] Even when the particle is not totally destroyed by heating, softened glass cannot maintain void structures once created by the moving particle.[17,18] To overcome this difficulty, laser modification assisted by chemical etching is promising.

View Article Online
DOI: 10.1039/C6NR06543K

When Au NP-decorated glass substrates were exposed repeatedly to irradiations of a nanosecond laser beam with a wavelength of 532 nm, material modification was found to occur on the glass surface at the expense of fragmentation and evaporation of Au NPs. The modified areas were found susceptible to chemical etching by HF solution, forming craters.[19,20] In this respect, a technique involving femtosecond laser structuring has been established for transparent materials, without the aid of Au NPs. A near-infrared multi-photon absorption-induced material modification enabled a subsequent chemical etching by HF or KOH.[21–23] This technique, however, is limited in that it produces only microcavities and microchannels rather than nanostructuring primarily because of diffraction-limited optics and secondarily because of over etching beyond the modified areas.

In this study, we applied a protocol consisting of plasmonic heating-assisted modification of glass with simultaneous chemical etching of the modified area. For this purpose, a focused illumination of a continuous wave (CW) laser was used for a Au NP acting as a local heating source for glass substrates, and aqueous tetrabutylammonium hydroxide solution was used as a control etching reagent (Scheme 1). The CW laser heating is advantageous for this purpose over pulsed heating because high temperature can be maintained for a sufficient period of time to allow for simultaneous chemical etching. In pulsed irradiation, a high-temperature period for modification is quite limited aside from the fact that most of the photons are unabsorbed. In addition, the advantage of pulsed lasers, i.e., their high peak powers, cannot be fully exploited because pulsed illuminations tend to generate vapor bubbles and cause particle fragmentation[20] if not maintained under low intensity control. Plasmonic heating was also applied in this study to fabricate a nanodome encapsulating a Au NP on a glass substrate using a laser-induced accumulation/aggregation technique developed very recently.[24]

View Article Online
DOI: 10.1039/C6NR06543K

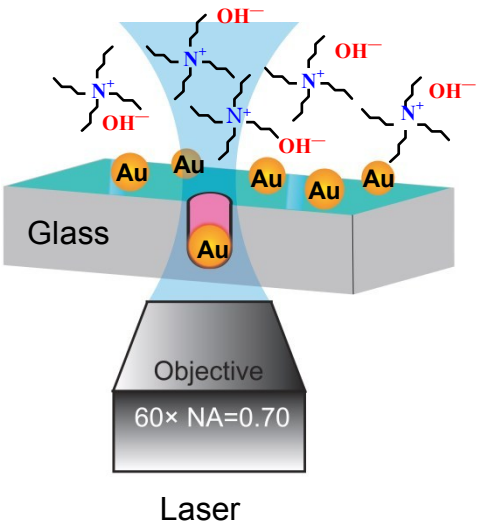

Scheme 1. Outline of the experiment.

View Article Online
DOI: 10.1039/C6NR06543K

Results and Discussion

Nanopores from laser-nanoparticle-assisted chemical etching

Single Au NPs supported on a borosilicate glass substrate and submerged in 40% (1.5 M) tetrabutylammonium hydroxide (TBAOH) solution were subjected to illumination with a focused laser beam with a wavelength of 488 nm that excites the intraband (LSPR) and interband transitions of the NPs. We employed the up beam to illuminate the two configurations, floor (I) and ceiling (II), given in Figure 1a. Figure 1b shows the overhead view of the scanning electron microscope (SEM) images that exhibit the effect of exposure to laser on the glass surfaces (floor illumination); images are shown before and after illumination of a Au sphere of diameter 104±5 nm (ESI, S1 for transmission electron microscopy image). We used a peak power density of 5.0 mW μm^{-2} (5.0×10^5 W cm^{-2}) that is below the melting threshold of the particle and simultaneous vapor bubble formation (~6 mW μm^{-2}). Before illumination (image I), the particle is seen supported on the glass surface. Remarkably, after illumination for 10 s, the Au sphere has sunk into the substrate, fitting just into a cavity (image II). After the particle was removed by sonication in water, the cavity has nearly the same diameter as the ejected Au sphere (image III). By increasing the irradiation period to 30 s (image IV, tilted) and 30 min (image V), deeper holes were fabricated; the particle is seen in image IV but not in image V. These results clearly show that nanoholes were fabricated on the glass surface just underneath the particle by laser illumination. Note that for post-mortem SEM imaging, each irradiated spot was located in reference to marks patterned on the substrates using a focused ion beam (FIB).

We looked at the effect of particle shape on the nanohole fabrication. Figure 1c shows the overhead SEM images when Au nanotriangles were used instead of Au nanospheres. Interestingly, we observed nanoholes with a triangular face. In image I, we irradiated for just 3 s at 3.3 mW μm^{-2}

View Article Online
DOI: 10.1039/C6NR06543K

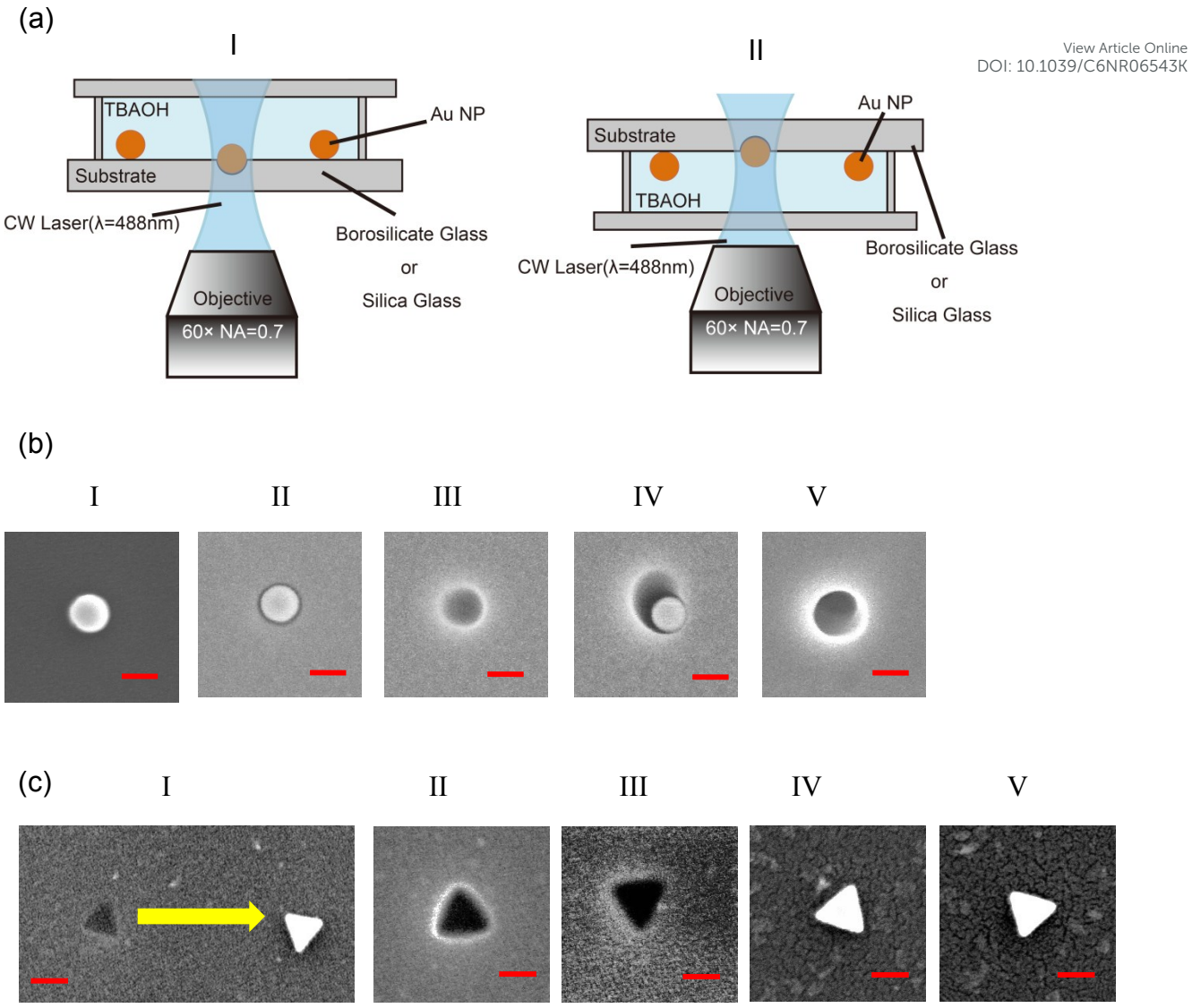

Figure 1. (a) Experimental configuration: I, floor illumination; II, ceiling illumination. (b) SEM 2D images showing the effect of laser illumination (floor illumination configuration) with a peak power density of 5.0 mW μm^{-2} on 100-nm-diameter Au nanospheres supported on a glass substrate; I, before irradiation (Au NP is sitting on the substrate surface); II, 10 s of irradiation (Au NP is fallen into a hole); III, 10 s of irradiation and Au NP removed by sonication; IV, 30 s of irradiation (tilted image; Au NP is seen at the bottom); V, 30 min of irradiation (Au NP is far inside the hole and could not be seen). (c) SEM images of laser irradiated Au nanotriangles supported on a glass substrate (floor illumination configuration); I: after irradiation at 3.3 mW μm^{-2} for 3 s and a nanotriangle was incidentally dislocated; II: after irradiation for 60 s at 3.3 mW μm^{-2}; III: after irradiation at 180 s at 3.3 mW μm^{-2}; IV: after irradiation for 10 s at 1.7 mW μm^{-2}; V: after irradiation for 300 s at 1.7 mW μm^{-2}. All scale bars represent 100 nm.

View Article Online
DOI: 10.1039/C6NR06543K

and observed unexpectedly both a triangular hole, which appears to be shallow, and a Au nanotriangle, which was originally supposed to be in the hole but has been displaced. By increasing the illumination periods, deeper holes were fabricated: in image II, after 60 s, and in image III, after 180 s. Both images do not show figures ascribable to Au triangles because they had sunk further inside the substrate. This assumption was confirmed by a dark-field microscopy (see below). However, when illuminated at lower laser intensities, for instance, at 1.7 mW μm^{-2}, one-half that used for images II and III, we could see Au nanotriangles sitting in the glass surface in images IV and V. In these instances, we assume no holes were fabricated on the glass surface, suggesting that a threshold laser intensity exists for nanohole fabrication (this will be detailed below). Moreover, besides borosilicate glass, nanoholes were fabricated on silica glass alike (ESI, S2).

For *in-situ* monitoring of the NP embedding process, we recorded white-light scattering spectra of a Au NP after certain periods of irradiation. These spectral measurements were performed by interrupting the laser illumination. Figure 2a shows the spectral changes of laser-irradiated period-dependent scattering for the LSPR band of a Au nanosphere of 100-nm diameter. We observed gradual red shifts with a slight broadening of the spectral envelope. From the time-dependent peak wavelengths an appreciable redshift of ~8 nm occurred in 10 s of illumination and stayed nearly constant later (Figure 2b and 2c). The LSPR red shifts along with spectral broadening are usually ascribed to an increase in the refractive index of the medium sensed by the Au NP.[25,26] Given that the refractive index of 40% aqueous TBAOH is 1.405 and that of Schott D 263T glass is 1.52, the observed red shifts are well-correlated with the embedding of Au NP into the glass substrate (Figure 2d). To confirm this assumption, we performed a numerical simulation using COMSOL Multiphysics of the LSPR scattering cross section spectrum varying the embedding depth. As expected, the simulation result (Figure 2e) suggests that the embedding of a Au sphere results in spectral broadening and redshifts consistent with experimental observations.

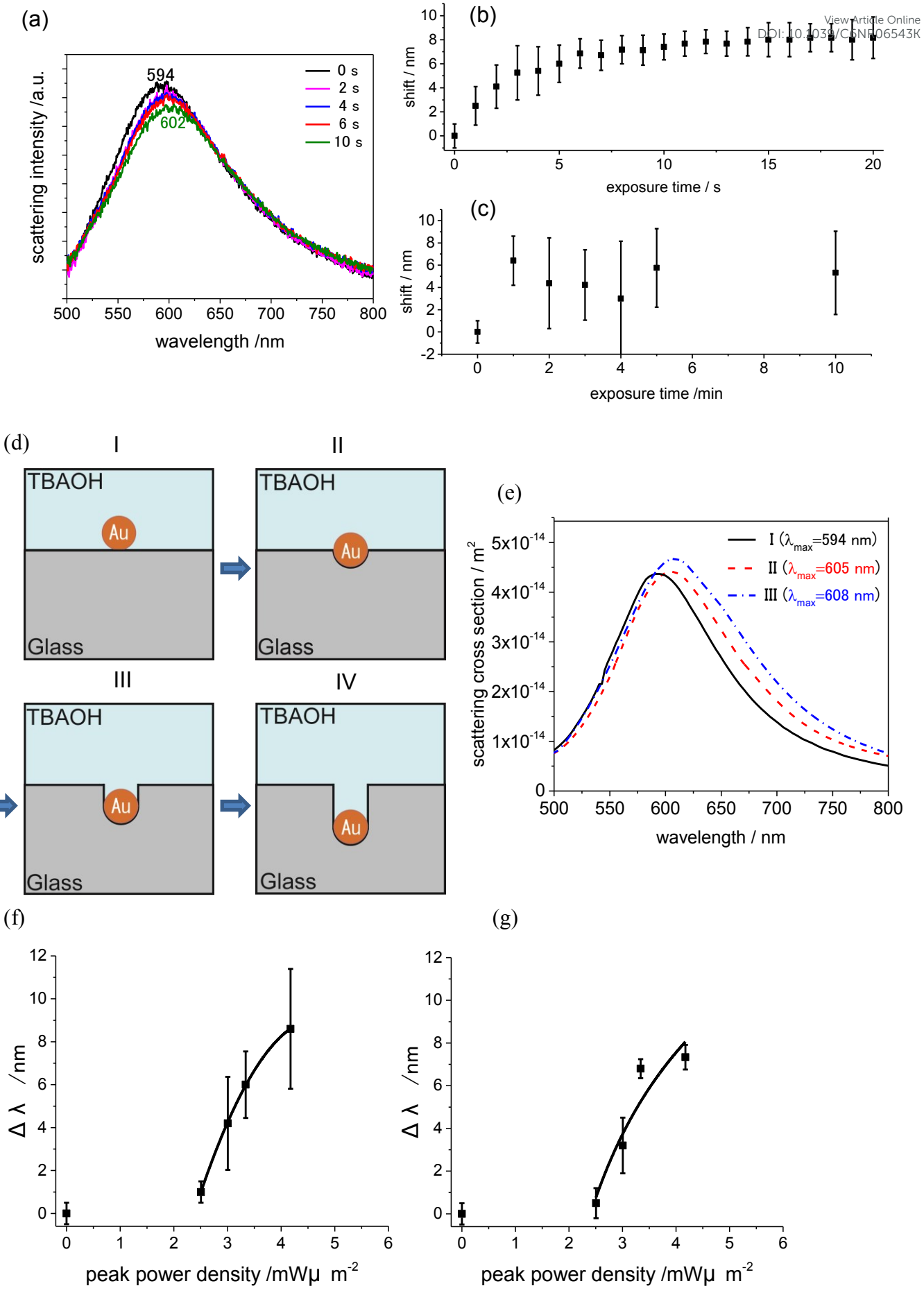

Figure 2. (a) Spectral changes of laser-irradiated period-dependent scattering of a 100-nm-diameter Au NP submerged in 40% TBAOH. (b) Scattering spectral peak shift as a function of exposure time at a shorter timescale. (c) Scattering spectral peak shift as a function of exposure time at a longer timescale. For (a)–(c), laser peak power density is 3.3 mW μm^{-2}. (d) Schematic representation of the laser-induced embedding of a Au NP into a glass substrate. (e) Simulated scattering spectra for a 100-nm-diameter Au NP resulting from embedding into a glass substrate (medium: aqueous TBAOH). Numbers I, II and III correspond to the geometries given in (d). The spectral simulation was performed using COMSOL Multiphysics 5.2a (http://www.comsol.com). Laser intensity dependence of the scattering spectral peak shift after 5 s of illumination in (f) the floor configuration and (g) the ceiling configuration.

View Article Online
DOI: 10.1039/C6NR06543K

Experimentally, the scattering intensity decreased with Au NP embedding (Figure 2a), which is slightly different from the simulation given in Figure 2e. This is because the focal area of the objective collecting scattered light remains on the glass surface, whereas the Au NP gradually moves out of focus as it bores into the glass. From the time-dependent spectral measurement, we conclude that the spectral shift in particle scattering used in estimating the embedding depth into the substrate is only applicable at the initial stage. Notably, changes in spectral scattering following nanoparticle embedding were observed also for the Au nanotriangles (ESI, S3).

At this point, we acquired cross-sectional images of nanoholes to investigate their shape and depth. For this purpose we used SEM assisted by focused-ion-beam (FIB) processing. Figure 3a and 3b shows the sectional image fabricated by the FIB for embedding Au spheres. Figure 3a shows an L-shaped channel as visualized through the glass wall (dark area in the center). Further milling of the wall removed the channel structure. A bent channel was unexpected as we presumed the particle would advance through glass etching at the particle–glass contact area beneath the particle. Uncertainty in the etching direction may arise, however, through either inhomogeneity in the glass material or imperfect sphericity of the Au NP. Besides the presence of an entrance in Figure 3b, a portion of an embedded Au nanosphere is illuminated as a bright spot in the center of a hole deep within the substrate, although no channel structure is evident. The FIB box milling has caused melting of the glass surface and the entrance of the nanohole has been deformed under expansion. The channel structure possibly bends here again making the whole structure difficult to show. Nevertheless, we verified that the Au NP was actually embedded inside the channel. We estimated the length of the nanohole from the entrance to the particle to be 0.8 μm after illumination for 5 min at 3.3 mW μm^{-2}, taking the tilt angle of 60° in SEM acquisition into consideration. For nanotriangles, we see a slit-like channel structure (Figure 3c) but not the base plane. At a shorter etching time, we are able to see the base plane of a hole (Figure 3d) but the Au nanotriangle was lost. At this stage, acquiring the illumination time *vs*. depth relationship is technically difficult, although such information is vital to show the advantages and limitations of the current method.

View Article Online
DOI: 10.1039/C6NR06543K

For nanohole fabrication with 100-nm-diameter spheres, we estimated the threshold laser intensity for both the floor and ceiling configurations by measuring scattering spectral peak shifts after 5 s of illumination (Figure 2f and 2g). This threshold was 2.5 mW μm^{-2} for both configurations. The result may suggest that the effects of gravity and scatting force that pushes Au NP in the forward direction[27] are negligible for particle burrowing (ESI, S4 for illumination in the ceiling configuration). Instead, the capillary effect of water moving into the narrow space between particle and substrate can play a role in embedding the particle.

To fabricate deeper nanoholes, the particle had to be forcefully embedded using an optical manipulation technique. Although it was not feasible to manipulate a Au NP embedded vertically, it was possible to move a particle horizontally (Figure 4). We first illuminated a Au NP (orange spot at the center) supported on a glass substrate (Ia) in the floor configuration and the particle was embedded after 40 min (Ib). The overhead light scattering image shows that the particle position (orange spot) is slightly shifted from the nanohole entrance (circled), possibly because the nanohole is fabricated with a slant. We then slowly moved the laser focus (d ~1 μm) horizontally near the particle embedded. We observed the particle had been displaced in the direction away from laser focus, 2 μm from the entrance after 120 min of illumination (Ic). In this case, we assume that the scattering force from the laser beam acts to move the particle horizontally.[14] The lower panels in Figure 4 illustrate the progressive etching observed in the upper panels. Further sophistication using a diffraction-limed optics and a 3D piezo stage is necessary for better manipulation.

View Article Online
DOI: 10.1039/C6NR06543K

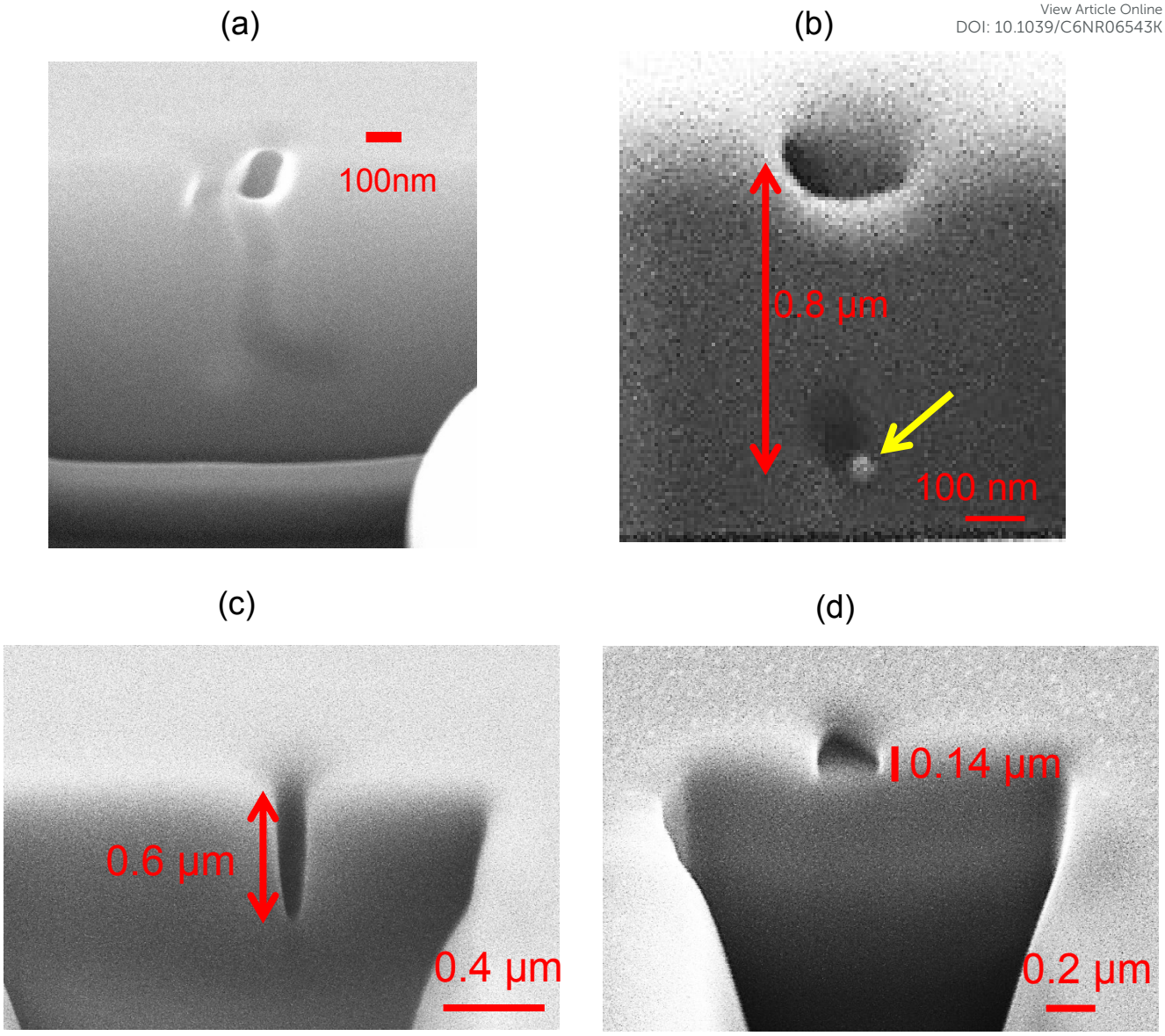

Figure 3. Cross-sectional SEM images. The section was created by the FIB box milling of the glass surface next to the nanohole. (a) An L-shaped nanochannel (dark area) captured through the glass wall by applying an electron acceleration voltage of 30 kV at a 45° tilt. Fabrication: illumination for 10 min at 3.3 mW μm^{-2}. (b) A nanohole entrance and an embedded Au nanosphere (yellow arrow) after illumination for 5 min at 3.3 mW μm^{-2} (60° tilted). The nanohole entrance is deformed and expanded from the original size because of melting from heat generated during the FIB milling. The nanosphere was seen but the sectional profile of the nanohole was not seen as it is hidden from view inside the glass wall. (c) A nanohole prepared by irradiating a nanotriangle for 30 min at 3.3 mW μm^{-2} in TBAOH (45° tilted). The base is not seen. (d) A nanohole prepared from a nanotriangle by irradiating for 5 min at 3.3 mW μm^{-2} in TBAOH (45° tilted). The nanotriangle was lost during the milling. Instead, the base plane was shown. The electron acceleration voltage for SEM acquisition is 5 kV for (b) ~ (d).

View Article Online
DOI: 10.1039/C6NR06543K

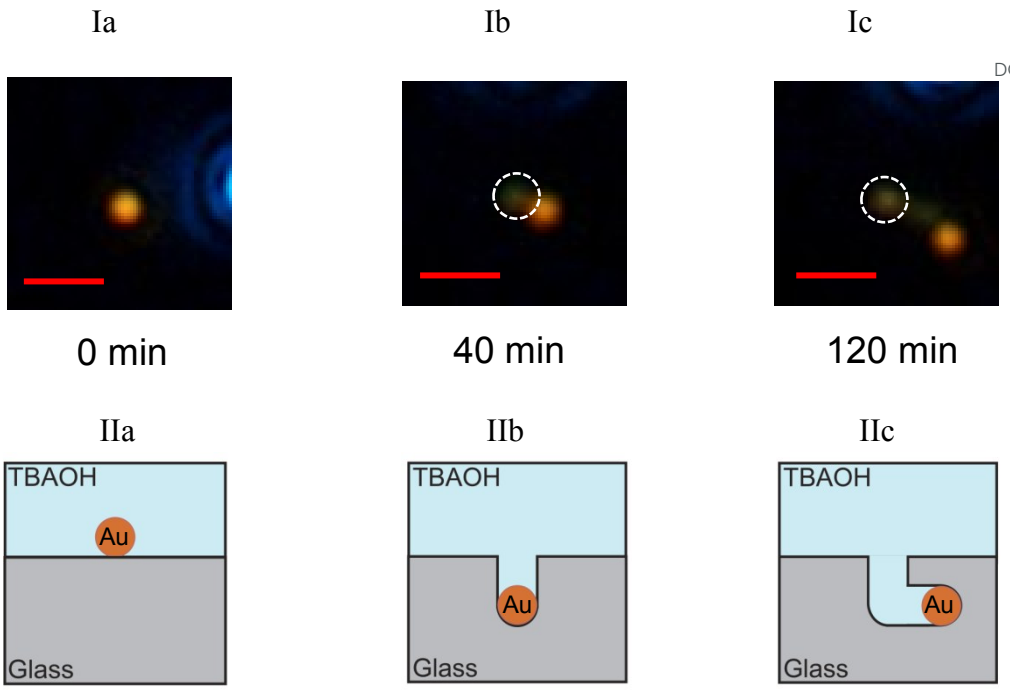

Figure 4. Upper panels show the dark-field optical microscope images of the steps to extend the nanohole horizontally by manipulating a Au NP using the laser focus spot. First, a Au NP, (orange spot at the center of Ia) supported on a glass substrate was embedded with focused laser illumination of intensity 3.3 mW μm^{-2} for 40 min. In Ib, the Au NP is embedded in the substrate; the weak scattering spot (circled) next to the Au NP is the nanohole entrance. After embedding, the Au NP is slightly shifted from the entrance. The laser focusing spot was moved horizontally in small steps; after 120 min (Ic), we see the Au NP is 2 μm from the nanohole entrance (circled). The scale bars represent 2 μm. Lower panels show a schematic illustrating the steps observed in the upper panels.

View Article Online
DOI: 10.1039/C6NR06543K

Etching mechanism

Certain information regarding the laser modification that allowed the post-etching of glass is available in the literature, in particular, for silica glass. For instance, the photo-modification of glass through multi-photon absorption from a femtosecond infrared laser beam enabled chemical etching with HF and KOH forming microchannels.[21–23] The susceptibility to etching acquired by the silica glass was ascribed to densification represented by increased fictive temperatures and the increased number of unstable three- and four-membered ring structures of –O–Si–O– bonds in the irradiated area compared with intact areas that are composed mainly of stable six-membered ring structures.[28] The deduction was based on IR and Raman spectroscopies.[29,30] For the irradiation using nanosecond laser pulses of a Au NP-assembled surface of borosilicate and silica glass with a wavelength of 532 nm, it was found that the area irradiated was vulnerable to etching by aqueous HF solution; this was also ascribed to laser heating-induced structural modification of the glass surface because heat transfer from the particle causes temperature increases in the glass surface.[19] For CW laser irradiation, Hidai and coworkers observed the modification and susceptibility to etching by HF of both borosilicate and silica glasses when coated with a metal film (Cu, stainless) on one side and irradiated from the other side to the metal film at a wavelength of 514 nm with power densities of ~10^6 W cm^{-2} or 10 mW μm^{-2}.[31,32] In this case, the modification occurred along the photophoretic migration of melt metal nanoparticles toward the direction of the laser source.[18] The Hidai group ascribed the mechanism of HF susceptibility to the modification caused by rapid heating and quenching of glass materials based on the measurement of Raman spectra for silica.[31,32] These results suggest that laser-induced heating can result in structural modification that leads to increased conformity to chemical etching regardless if pulsed or CW laser illuminated.

In our experiment, the heating of the glass substrate occurred through contact heat transfer from Au NP. For CW laser illumination of a Au NP, steady-state particle temperatures can be reached quite rapidly within less than a microsecond of exposure.[33] This rapid heating is important for the modification of glass structures.[31,32] According to the temperature simulation using

View Article Online
DOI: 10.1039/C6NR06543K

COMSOL Multiphysics, the steady-state particle temperatures reached are estimated to be 400–480 K for laser peak power densities, 3.3–5.0 mW μm^{-2}, considering heat dissipation to the medium and substrate (ESI, S5). In the steady-state illumination, the adjacent medium to the particle has approximately the same temperature as the particle under illumination.[34] Hence the estimated temperature of the glass surface is not surprisingly high, but efficient etching of 0.8 μm after illumination for 5 min at 3.3 mW μm^{-2} by TBAOH in fact proceeded. In alkali etching of glass, $[OH^-]$ plays a crucial role for facile processing. In this regard, we remark that the ion product of water, K_w is temperature-dependent. As temperature increases from 298 K to 400 and 480 K, K_w increases from $10^{-14.0}$ to $10^{-11.9}$ and $10^{-11.2}$. [35] The resulting higher $[OH^-]$ should increase the etching rate of glass remarkably. In our experiment of Au NP heating, no vapor bubbles formed, as described above. The generation of nano- and microbubbles in a liquid has been shown to occur around plasmonic NPs under CW laser illumination.[36–38] The local temperature required to trigger bubble generation, though, is much higher than the boiling point of water under 1 atm (100°C, 373 K), because of the presence of Laplace pressure. Bubble nucleation was reported to occur in superheated water with threshold particle temperatures between 220 and 240°C (493–513 K). [35–37]

In comparison, with the laser-assisted etching of glasses described here, a comment on the homogeneous (oven) heating-induced embedding of Au NPs into SiO_2 glass is given. de Vreede and coworkers demonstrated that Au particles with initial 1-μm diameter and 18-nm thickness were buried into the SiO_2 glass when heated to 1050°C (1323 K), leaving nanoholes.[17] After 9 hours of heating, a nanohole with a depth of 0.8 μm was formed and a Au NP diameter was reduced to 25 nm. Apparently, the evaporation of Au NP occurred during the process because the temperature is close to the melting point of Au, 1064°C (1337 K). The driving force of the embedding was ascribed to a continuous evaporation of Au transporting SiO_2 to the surface and leading to ridge formation. In a practical sense, their method suffers from slow processing, unfavorable ridge formation, and the narrowing of the channel diameter with depth. For the purpose of nanohole fabrication, our method is free from these shortcomings. Interestingly, according to Hidai and

View Article Online
DOI: 10.1039/C6NR06543K

coworkers,[18] migration of metal particles occurred but no holes were left when a system similar to that used by de Vreede and coworkers was illuminated with a CW laser from the opposite side of the glass substrate. In this case, a liquid droplet of a metal moved inside the glass toward the laser direction while softening the glass ahead of the moving particle without leaving a void space behind it because of rapid cooling in the ambient temperature.

Instead of glass, pore fabrication on the (100) face of silicon wafer has been known for years through oxidative etching in aqueous HF/H_2O_2 solution using metal micro- and nanoparticles (Au, Pt, Ag) as a catalyst.[39–41] In this case, the chemical treatment can be done at ambient temperature without light illumination. The etching rate was remarkably fast (~30 μm per 50 min for Au).[39] In our fabrication, laser illumination is the essential part of the technology to trigger and terminate fabrication, and have control over etching rates. Additionally, embedding of Au NPs into glass can be monitored *in situ* through optical measurements as demonstrated earlier.

Laser-induced nanodome fabrication.

When a single Au nanosphere supported on a borosilicate glass substrate was subjected to a laser illumination in 40% aqueous TBAOH solution that was left in contact with the glass surface for 10 hours, we observed progressive red shifts in the LSPR scattering spectra with increasing laser illumination period (Figure 4a). Moreover, remarkable broadening and intensity enhancement were seen. The spectral changes are reminiscent of LSPR that responds to the gradual increase in refractive index of the surrounding medium.[25,26] To determine the origin of the spectral shifts, we acquired SEM images of 100-nm-diameter Au NPs under investigation. In Figure 4b, image I represents a non-irradiated bare Au sphere, whereas images II and III show a Au nanosphere after 10 minutes of irradiation.

View Article Online
DOI: 10.1039/C6NR06543K

(a)

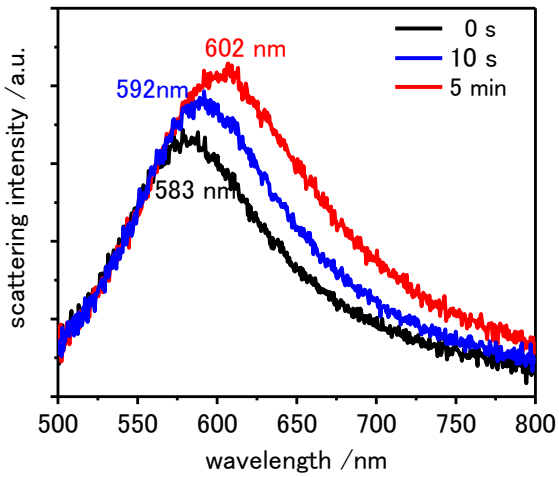

(b)

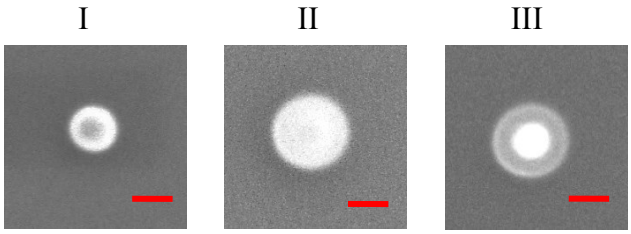

(c)

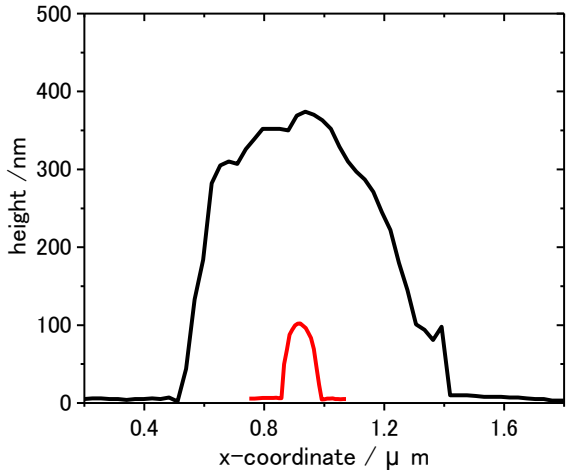

Figure 5. (a) The laser illumination period-dependent scattering spectral changes of 100-nm-diameter Au nanosphere submerged in 40% aqueous TBAOH solution and left for 10 h. Laser peak power density: 3.3 mW μm^{-2}. (b) 2D images representing nanodome fabrication on a glass substrate: I, an original Au nanosphere; II, a particle after 5 minutes of irradiation at 3.3 mW μm^{-2} imaged with the electron acceleration voltage of 3 kV; III, the same particle (after 5 minutes of irradiation) imaged with the acceleration voltage of 10 kV. Scale bars represent 100 nm. (c) AFM height profiles: red line, 100-nm-diameter bare Au nanosphere; black line, after irradiation at 3.3 mW μm^{-2} for 60 minutes.

View Article Online
DOI: 10.1039/C6NR06543K

These two images are of the same particle but imaged at different electron acceleration voltages of 3 and 10 kV. A comparison of the two images clearly shows that a nanodome is formed from the embedding of an Au nanosphere as a result of laser illumination. Evidence for the nanodome was obtained from the AFM height profile (Figure 4c). For non-irradiated bare Au NP, a height of 100 nm corresponding to the diameter of the Au nanosphere was recorded. In contrast, after irradiation at 3.3 mW μm^{-2} for 60 minutes, a height of ~350 nm was obtained, suggesting the formation of a thick shell. Moreover, the numerical simulation of scattering cross-section spectra using COMSOL Multiphysics gave a shell thickness-dependence of shift similar to that from experiment (ESI, S6).

Here we consider the encapsulation mechanism. The observation is reminiscent of the recent study by Enders and coworkers, who demonstrated the encapsulation of Au NP by polyethylene glycol and sodium dodecyl sulfate, forming a gold core–organic shell structure on laser heating of Au NP supported on a sapphire substrate.[24] They ascribed its origin to a capillary-induced phase separation of polymers, assisted by Marangoni convective flow that is generated by a surface-tension gradient formed along the hot Au NP to the cool substrate. In the present system, the shell is formed presumably from glass materials that were dissolved homogenously from the glass surface into the TBAOH solution when the solution had been in contact with the glass surface for 10 hours. The dissolved glass materials may form a colloidal solution. The encapsulation can be understood in analogy with glass formation through the sol-gel process.[42] When the particle temperature increases because of laser illumination, the gelation of colloids may proceed on a hot NP surface, leading to a shell around the NP. Under our experimental conditions, the particle temperatures are estimated to be from 400 and 480 K for laser peak power densities, 3.3–5.0 mW μm^{-2} (ESI, S5). Such temperatures are not sufficient for forming glass that needs 700–800 K but may suffice in promoting polymerization resulting in gel formation.

DOI: 10.1039/C6NR06543K

Conclusion

We demonstrated the nanofabrication of holes on glass surfaces applying a method of indirect heating of the glass surface through laser illumination of gold nanoparticles simultaneously with *in situ* chemical etching. The method is versatile in directing the size and shape of nanoholes, and thus opens up a new surface patterning strategy at the nanoscale. Furthermore, we define this achievement as a milestone in our strategic goal of the nanoscale through-hole structuring on ~100-μm-thick glass substrates. To realize this task, technical sophistication is required to optically trap nanoparticles, to locate particle position readily, and to execute precise control over laser focusing while etching is in progress. The current research is proceeding further along this line. We also fabricated a nanodome around a single gold nanoparticle supported on a glass substrate by a laser-heating-induced accumulation technique. In the fabrication of nanoholes and nanodomes, the CW laser illumination constitutes an important part of our optical heating-based technique in terms of improved throughput compared with the multiphoton-induced processing.

View Article Online
DOI: 10.1039/C6NR06543K

Experimental Methods

Sample Preparation. Aqueous solutions of Au nanospheres with nominal diameters of 100 nm (EMGC100) were obtained from BBI Solutions, Cardiff, UK. The particles were synthesized using a variation on the Frens citrate reduction method, and were stabilized with citrate.[43] Au NPs were transformed from faceted to spherical shape by irradiating with weak-intensity nanosecond laser pulses (~11 mJ cm^{-2}) of 532-nm wavelength. The particle image acquired using a transmission electron microscope and the corresponding size distribution (104±5 nm) are given in the ESI, S1. Au nanotriangles were synthesized according to the literature (see ESI, S1 for a SEM image).[44] The Au NPs were spin-coated onto an 18-mm × 18-mm × 0.5-mm borosilicate glass substrate (Schott D263T, Matsunami Glass, Osaka, Japan) or silica glass (VIOSIL, Shin-Etsu Chemical Co., Tokyo, Japan) cleansed just before use in a boiling mixture of 1:1 30% H_2O_2–28% ammonia mixture for 90 min. Then the Au NPs were washed three times with double-distilled water by placing 0.5 mL of water on a spin coater and spun. Au NPs on the glass slide were immersed in 40% (1.5 M) tetrabutylammonium hydroxide (Tokyo Kasei Co., Tokyo, Japan) solution in a 90-μL chamber consisting of two glass substrates sandwiched with a 0.2-mm-thick silicone rubber spacer.

Experimental Setup. A microscopy-spectroscopy setup was used for selecting a single Au NP, illuminating a focused laser beam, and measuring the progress of embedding or encapsulation through the Rayleigh scattering spectral changes. A halogen lamp with a broad spectrum was used for illumination when recording the scattering spectra. The particles were brought to the laser spot by scanning with a sample chamber on a motorized stage, BIOS-105T (SIGMA KOKI, Tokyo, Japan; 100-nm resolution). The particles were heated by illuminating a focused 488-nm CW laser, OBIS-488-LX-150 (Coherent, Santa Clara, CA) beam through a microscope objective (60×, NA = 0.70) on an inverted microscope, IX-71 (Olympus Co., Tokyo, Japan; with a dark-field condenser NA = 0.8 to 0.92). Two configurations were used: Au NPs sitting on the floor of the chamber and ones staying on the top wall (ceiling) of the chamber were subjected to laser illumination. The irradiation periods were regulated using an F77 mechanical shutter (SURUGA SEIKI, Tokyo,

View Article Online
DOI: 10.1039/C6NR06543K

Japan). The 488 nm laser light excites both interband and intraband transitions (see ESI S7 for the absorption spectrum of 100 nm-diameter Au sphere). Note, however, that the consequence of the both excitations is the same: hot electron generation and particle heating.[7] The temperature increase of an Au NP occurs simultaneously with opening the shutter and the temperature decrease follows immediately after closing the shutter.[33] The microscope has two ports. One leads to a SP-300*i* polychromator (Acton Research Co. MA with a grating of 150 grooves/mm blazed at 500 nm) with a DU401-BR-DD CCD camera (Andor Technology, Belfast, UK; operated at −60°C) through a 300-μm-diameter pinhole (view area: 5-μm diameter). The single particle scattering spectra were measured at a wavelength resolution of 0.5 nm. The spectra were obtained by subtracting the background signals of the surrounding media, then dividing it by the spectral profile of the white-light excitation source. The other port is used for particle imaging with a DS-5M digital camera (Nikon Co., Tokyo, Japan). A PD 300-UV photodiode power meter (Ophir Optronics Ltd., Jerusalem, Israel) was used to measure the laser intensity. The spatial laser profile was determined from scattering-signal intensity measurements from the laser spot while rastering the stage at 100-nm intervals. The laser beam diameter thus determined was 1.0 μm although a calculated $1/e^2$ diameter of 0.5 μm was obtained assuming a Gaussian beam profile and using experimental optical parameters (NA = 0.70, λ = 488 nm, n = 1.33). The laser peak power density I_p (mW μm^{-2}) was estimated assuming a Gaussian spatial profile. To ensure that the spectral measurements were always taken under the same conditions and to control the shape of the focal spot, the laser beam was brought into focus on the substrate surface at a distance 3–5 μm from the particle of interest before being positioned to illuminate the particle.

A field-emission scanning electron microscope, SEM S4700 (Hitachi High-Technologies Co., Tokyo, Japan) was used for imaging the glass surfaces and cross sections, on which Au was sputter-deposited. A thickness was determined to be 2–3 nm by measuring the thickness of the film at various locations on the glass substrate. For post-mortem SEM imaging, each single Au NP irradiated or nanohole was located using marks patterned on the substrates. For imaging the cross

section of the glass, focused ion beams (FIB) of Ga from JEM-9320FIB (JEOL Ltd., Tokyo, Japan) were used (acceleration voltage: 30 kV). The cross section of the glass was exposed by the box milling technique. Topographical (3D) images were acquired with the atomic force microscopy (AFM) on a NanoWizard II (JPK Instruments AG, Berlin, Germany) with a probe tip of a radius of curvature of 7 nm and spring constant of 2 $N \cdot m^{-1}$, OMCL-AC160 (Olympus Co., Tokyo, Japan).

Acknowledgments

Financial support from JSPS KAKENHI (No. 26286004) is gratefully acknowledged. We thank Tomoyuki Ueki for his technical support in SEM imaging. We thank Dr. Takayuki Uwada of Josai University for stimulating discussions.

References

1. U. Kreibig and M. Vollmer, *Optical Properties of Metal Clusters*; Springer: Berlin 1995.
2. J. N. Anker, W. P. Hall, O. Lyanders, N. C. Shah, J. Zhao and R. P. Van Duyne, *Nature Mat*. 2008, **7**, 442–453.
3. K. M. Mayer and J. H. Hafner, *Chem. Rev*. 2011, **111**, 3828–3857.
4. P. Wang, B. Huang, Y. Dai, and M-H. Whangbo, *Phys. Chem. Chem. Phys.* 2012, **14**, 9813−9825.
5. X. Zhang, Y. L. Chen, R-S. Liu and D. P. Tsai, *Rep. Prog. Phys*. 2013, **76**, 046401.
6. E. S. Arinze, B. Qiu, G. Nyijesy and S. M. Thon, *ACS Photonics*, 2016, **3**, 158–173.
7. M. L. Brongersma, N. J. Halas and P. Nordlander, *Nature Nanotech*. 2015, **10**, 25–34.
8. A. O. Govorov, and H. H. Richardson, *Nano Today*, 2007, **2**, 30–38.
9. Z. Qin and J. C. Bischof, *Chem. Soc. Rev.* 2012, **41**, 119–1217.
10. D. Boyer, P. Tamarat, A. Maali, B. Lounis and M. Orrit, *Science*, 2002, **297**, 1160–1163.
11. A. Gaiduk, P. V. Ruijgrok, M. Yorulmaz and M. Orrit, *Chem. Sci.*, 2010, **1**, 343–350.
12. V. Kotaidis, C. Dahmen, G. von Plessen, F. Springer and A. Plech. *J. Chem. Phys.* 2006, **124**, 184702.
13. E. Lukianova-Hleb, Y. Hu, L. Latterini, L. Tarpani, S. Lee, Drezek, R. A. J. H. Hafner and D. O. Lapotko, *ACS Nano* 2010, **4**, 2109–2123.
14. M. Fedoruk, A. A. Lutich and J. Feldmann, *ACS Nano*, 2011, **5**, 7377−7382.
15. M. Fedoruk, M. Meixner, S. Carretero-Palacios, T. Lohmüller and J. Feldmann, *ACS Nano*, 2013, **7**, 7648–7653.
16. T. Numata, H. Tatsuta, Y. Morita, Y. Otani and N. Umeda, *IEEJ Trans. Electr. Electron. Eng*. 2007, **2**, 398–401.
17. L. J. de Vreede, A. van den Berg and J. C. T. Eijkel, *Nano Lett*. 2015, **15**, 727−731.
18. H. Hidai, T. Yamazaki, S. Itoh, K. Hiromatsu and H. Tokura, *Opt. Express*, 2010, **18**, 20313.

19. S. Hashimoto, T. Uwada, M. Hagiri, H. Takai and T. Ueki, *J. Phys. Chem*. C 2009, **113**, 20640–20647.

20. S. Hashimoto, D. Werner and T. Uwada, *J. Photochem. Photobiol. C*, 2012, **13**, 28–54.

21. A. Marcinkevičius, S. Juodkazis, M. Watanabe, M. Miwa, S. Matsuo, H. Misawa and J. Nishii, *Opt. Lett*. 2001, **26**, 277–279.

22. S. Kiyama, S. Matsuo, S. Hashimoto, Y. Morihira, *J. Phys. Chem*. C 2009, **113**, 11560−11566.

23. R. Osellame, H. J. W. M. Hoekstra, G. Cerullo, and M. Pollnau, *Laser Photon. Rev*. 2011, **5**, 442–463.

24. M. Enders, S. Mukai, T. Uwada and S. Hashimoto, *J. Phys. Chem. C*, 2016, **120**, 6723–6732.

25. S. Underwood and P. Mulvaney, *Langmuir*, 1994, **10**, 3427–3430.

26. M. M. Miller and A. A. Lazarides, *J. Phys. Chem. B*, 2005, **109**, 21556–21565.

27. S. Nedev, A. S. Urban, A. A. Lutich and J. Feldmann, *Nano Lett*. 2011, **11**, 5066–5070.

28. K. Awazu and H. Kawazoe, *J. Appl. Phys*. 2003, **94**, 6243–6262.

29. A. Agarwal and M. Tomozawa, *J. Non-Cryst. Solids* 1997, **209**, 166–174.

30. Y. Bellouard, E. Barthel, A. A. Salid, M. Dugan and P. Bado, *Opt. Express*, 2008, **16**, 19520–19534.

31. H. Hidai, M. Yoshioka, K. Hiromatsu and H. Tokura, *Appl Phys A*, 2009, **96**, 869–872.

32. H. Hidai, M. Yoshioka, K. Hiromatsu and H. Tokura, *J. Am. Ceram. Soc*., 2010, **93**, 1597–1601.

33. P. Keblinski, D. G. Cahill, A. Bodapati, C. R. Sullivan and T. A. Taton, *J. Appl. Phys.*, 2006, **100**, 054305.

34. A. Siems, S. A. L. Weber, J. Boneberg and A. Plech, *New J. Phys*. **2011**, *13*, 043018.

35. W. L. Marshall and E. U. Frank, *J. Phys. Chem. Ref. Data*, 1981, **10**, 295–304.

36. Z. Fang, Y-R. Zhen, O. Neumann, A. Polman, F. J. Garcia de Abajo, P. Nordlander and N. J. Halas, *Nano Lett*. 2013, **13**, 1736−1742.

37. G. Baffou, J. Polleux, H. Rigneault and S. Monneret, *J. Phys. Chem. C* 2014, **118**, 4890–4898.

38. L. Hou, M. Yorulmaz, N. R. Verhart and M. Orrit, *New J. Phys*. 2015, **17**, 013050.

View Article Online
DOI: 10.1039/C6NR06543K

39. K. Tsujino and M. Matsumura, *Adv. Mater*. 2005, **17**, 1045–1047.

40. Z. Huang, N. Ceyer, P. Werner, J. de Boor and U. Gösele, *Adv. Mater*. 2011, **23**, 285–308.

41. G. Liu, K. L. Young, X. Liao, M. L. Personick and C. A. Mirkin, *J. Am. Chem. Soc*. 2013, **135**, 12196–12199.

42. L. L. Hench and J. K. West, *Chem. Rev*. 1990, **90**, 33–72.

43. G. Frens, *Nature Phys. Sci*., 1973, **241**, 20–22.

44. A. Mezni, T, Dammak, A. Fkiri, A. Mlayah, Y. Abid and L. S. Smiri, *J. Phys. Chem. C* 2014, **118**, 17956–17967.